PROCEEDINGS OF SPIE

SPIEDigitalLibrary.org/conference-proceedings-of-spie

3D FDTD analysis of cross-talk in pixelated PA-LCos devices: impact of fill factor and size pixel on S2 and S3 parameters

Jorge Francés, Adriana Sánchez, Andrés Márquez, Sergi Gallego, Mariela Álvarez, et al.

Jorge Francés, Adriana R. Sánchez, Andrés Márquez, Sergi Gallego, Mariela L. Álvarez, Inmaculada Pascual, Augusto Beléndez, "3D FDTD analysis of cross-talk in pixelated PA-LCos devices: impact of fill factor and size pixel on S2 and S3 parameters," Proc. SPIE 12673, Optics and Photonics for Information Processing XVII, 126730P (4 October 2023); doi: 10.1117/12.2676321

SPIE.

Event: SPIE Optical Engineering + Applications, 2023, San Diego, California, United States

3D FDTD analysis of cross-talk in pixelated PA-LCos devices: impact of fill factor and size pixel on S_2 and S_3 parameters

Jorge Francés[a,b], Adriana R. Sánchez[b], Andrés Márquez[a,b], Sergi Gallego[a,b], Mariela L. Álvarez[a,b], Inmaculada Pascual[b,c], and Augusto Beléndez[a,b]

[a]Departamento de Física, Ingeniería de Sistemas y Teoría de la Señal, Universidad de Alicante, P.O. Box 99, E-03080 Alicante, Spain
[b]I.U. Física Aplicada a las Ciencias y las Tecnologías, Universidad de Alicante, P.O. Box 99, E-03080 Alicante, Spain
[c]Departamento. de Óptica, Anatomía y Farmacología, Universidad de Alicante, P.O. Box 99, E-03080 Alicante, Spain

ABSTRACT

In the last decades, new technology fabrication developments have permitted increased resolution and reduced pixel size of Liquid crystal on silicon (LCoS) microdisplays. However, the pixel size reduction triggers the microdisplay performance degradation due to different phenomena, such as the cross-talk between neighbouring pixels, fringing fields, out-of-plane reorientation of the liquid crystal director, and diffraction effects due to the pixelated grid pattern of the microdisplay. In this work, a full 3D simulation model has been applied to predict the liquid crystal director orientation as a function of space and external voltage. The scheme here considered provides the complete vectorial information of the electromagnetic field distribution produced by one single pixel illuminated by plane waves circularly polarised. This analysis is carried on for several pixel and gap sizes for different external voltages. This research focuses on S_2 and S_3 Stokes parameters and how their behaviour is affected due to the cross-talk phenomena previously presented.

Keywords: Liquid Crystal, Stokes Parameters, cross-talk, fill factor

1. INTRODUCTION

In the last decades, new technology fabrication developments have permitted increased resolution and reduced pixel size of Liquid crystal on silicon (LCoS) microdisplays. As a result, LCoS are very popular in advanced photonic applications, e.g. phase-only modulation[1,2] and spatial light modulators.[3,4] However, the pixel size reduction triggers the microdisplay performance degradation due to different phenomena,[5] such as the cross-talk between neighbouring pixels, fringing fields, out-of-plane reorientation of the liquid crystal director, and diffraction effects due to the pixelated grid pattern of the microdisplay.[6–10] In this work, a full 3D simulation model has been applied to predict the liquid crystal director orientation as a function of space and external voltage. More precisely, the minimisation of the elastic free energy has been performed in 3D with a good enough resolution and considering the influence of the external voltage applied to the pixel electrodes. Once the liquid crystal director is estimated, the permittivity tensor is derived and provided to a full 3D vectorial simulation based on an ad-hoc finite-difference time-domain (FDTD) scheme.[11–14] Due to the high degree of detail required for the mesh in this stage, a full 3D GPU FDTD scheme has been developed. This step provides the complete vectorial information of the electromagnetic field distribution produced by one single pixel illuminated by plane waves circularly polarised. This analysis is carried on for several pixel and gap sizes for different external voltages. This research focuses on S_2 and S_3 Stokes parameters and how their behaviour is affected due to the cross-talk phenomena previously presented. Preliminary validations of the setup have been included in the work. After that, the results on PA-LCos show that the device's performance is more robust and stable for S_2 and S_3 parameters compared to S_1 and DOP. These results are consistent with previous analyses performed following this setup for other pixel sizes and fill factors.

Further author information: (Send correspondence to J. Francés)
J. F.: E-mail: jfmonllor@ua.es, Telephone: +34 96 590 9951

Optics and Photonics for Information Processing XVII, edited by Khan M. Iftekharuddin, Abdul A. S. Awwal, Victor Hugo Diaz-Ramirez, Proc. of SPIE Vol. 12673, 126730P · © 2023 SPIE · 0277-786X · doi: 10.1117/12.2676321

2. SIMULATION MODEL

To effectively model the light interactions in an LC-based SLM device, it is crucial to establish a precise orientation for the LC director. To determine the distribution of the LC director when subjected to an electric field **E**, we adopt the methodology outlined in previous works.[5,15,16] The objective of this approach is to identify a director configuration that minimises the overall Frank-Oseen free-energy density:

$$f = \frac{1}{2}K_{11}(\cdot\mathbf{n})^2 + \frac{1}{2}K_{22}(\mathbf{n}\cdot\nabla\times\mathbf{n})^2 + \frac{1}{2}K_{33}(\mathbf{n}\times\nabla\times\mathbf{n})^2) - \frac{1}{2}\boldsymbol{\epsilon}\mathbf{E}\cdot\mathbf{E}.$$

Let K_{11}, K_{22}, and K_{33} represent the elastic constants associated with splay, twist, and bend, respectively. The electric field inside the LC is denoted as **E**, and the dielectric tensor $\boldsymbol{\epsilon}$ characterises the LC material's properties concerning the director **n** through Eq.(2) in.[11] The minimisation of the free energy detailed in (1) is fully detailed in.[11,16] Table 1 summarises the parameters and values considered for the numerical simulations, where the liquid crystal parameters correspond to the well-known E7 compound.

Table 1. Parameter values used for numerical simulations.

Parameter description	Symbol	Value
Frank-Oseen elastic coefficients	K_{11}, K_{22}, K_{33}	12 pN, 9 pN, 19.5 pN
refractive indices LC	n_e, n_O	1.7646, 1.5289
relative dielectric permittivity	$\epsilon_{\parallel}, \epsilon_{\perp}$	19.6, 5.1
thickness of the LC-SLM	d_{LC}	2.9792 μm
maximum voltage	$\Phi_{\max}$	5 V

The grid density for the FDTD simulation is set at 20 points per wavelength, resulting in a fixed spatial resolution of 26.6 nm when considering the input wavelength of 532 nm. In order to comply with the Friederich-Levy-Courant condition, which limits the relationship between spatial and temporal resolutions,[17,18] the time interval is set at $\Delta t = 6.27 \times 10^{-17}$ seconds.

The simulation scheme implies spatially discretising a single LC-SLM pixel in a three-dimensional framework. Each point of this discretisation establishes the simulation grid, enabling the estimation of the LC director. The SF-FDTD method is employed[17,19] for solving Maxwell's equation. The LC director is set along the horizontal of the reference system, simulating right-handed circular polarisation, following the scheme on[11] and in.[20]

In this study, we analyze the fill factor, which is the percentage ratio between the active area of a pixel and its entire area, excluding the interpixel gap. The study examines pixel sizes of 3, 5, and 7 μm and analyzes the computed Stokes parameters, S_i, and degree of polarization, DOP, as a function of input voltage for various pixel sizes and interpixel gaps. Table 2 offers a summary of the cases used for these results.

Table 2. LC-SLM fill factor pixel considered for the simulations

d_{pixel}	d_{gap}=0.2 μm	d_{gap}=0.4 μm	d_{gap}=0.6 μm
3	87%	75%	64%
5	92%	85%	77%
7	94%	89%	84%

3. RESULTS

Fig. 1 shows the Stokes parameters as a function of the external voltage applied to the pixel for the different pixels considered and the interpixel gap (see Table 2). Specifically, Fig. 1(a)-(c) depicts the S_1 parameter for pixel sizes of 3, 5, and 7 μm, respectively. As the pixel size increases, the amplitude of the deviation of S_1 compared to the infinite case diminishes.

Additionally, enlarging the interpixel gap for each pixel appears to have a degrading effect on the pixel's performance, leading to an increase in the deviation of S_1. However, quantifying this effect proves to be more challenging.

Continuing with the same approach, Fig. 1(d)-(f) and Fig. 1(g)-(i) represents the S_2, and S_3 results, respectively. In these two sets of graphs, identifying deviations becomes difficult. Consequently, Fig. 2 compares the errors of these two parameters to the infinite pixel. Fig. 1(j)-(i) shows the DOP that is, in all situations, perfectly aligned to the infinite case. Here, coherent superposition of the Stokes parameters is considered to compute the averages of these parameters as a function of the space.

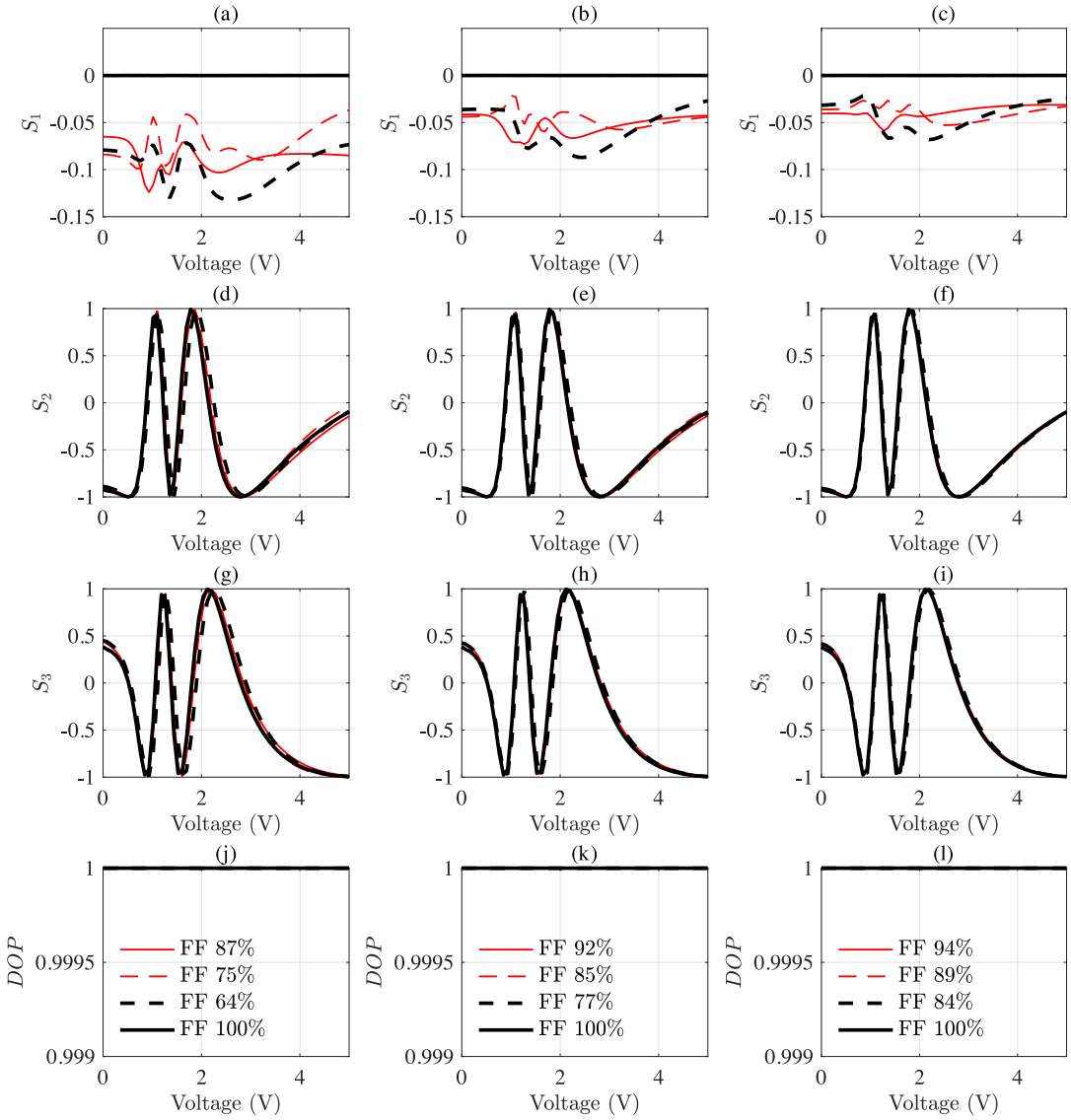

Figure 1. Representation of the Stokes parameter as a function of the voltage applied to the pixel. (a) S_1 for d_{pixel}=3 μm. (b) S_1 for d_{pixel}=5 μm. (c) S_1 for d_{pixel}=7 μm. (d) S_2 for d_{pixel}=3 μm. (e) S_2 for d_{pixel}=5 μm. (f) S_2 for d_{pixel}=7 μm. (f) S_3 for d_{pixel}=3 μm. (g) S_3 for d_{pixel}=5 μm. (h) S_3 for d_{pixel}=7 μm. (i) DOP for d_{pixel}=3 μm. (j) DOP for d_{pixel}=5 μm. (k) DOP for d_{pixel}=7 μm.

In Figure 2 (a)-(c), we can see the absolute error of the S_2 parameter for pixel sizes of 3, 5, and 7 μm. Similarly, in Figure 2 (d)-(f), we can observe the absolute error of the S_3 parameter for the pixel sizes under study. In all cases, we notice that the deviation from the infinite case decreases as the pixel size increases. The analysis highlights that the worst fill factor generally results in the highest deviations for each pixel. The two best fill factors seem to have a similar effect on deviations, with the best fill factor typically having a slightly better response in all cases. However, the impact of this effect on voltage shows significant variability in the region between 1-3 Volts. Notably, different pixel sizes with the same fill factor are not directly comparable, as they appear non-equivalent. In order to measure this effect, the average absolute error for each trace is included in the legend for each graph.

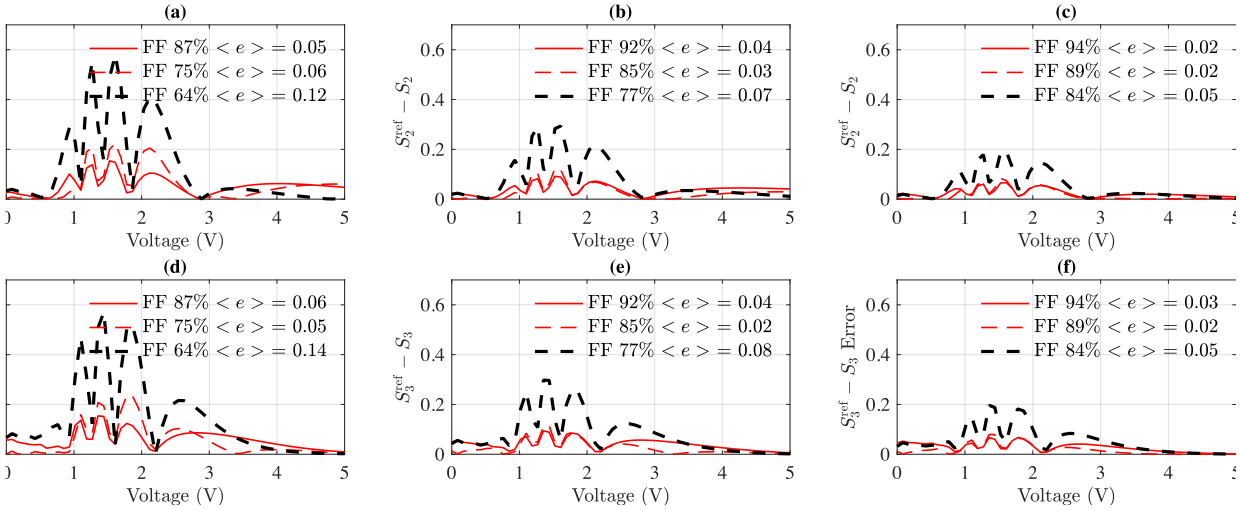

Figure 2. Absolute error between the infinite and finite pixel as a function of the voltage applied. The mean absolute error for each trace is included in the legend of each sub-graph. (a) $|S_2^{ref} - S_2|$ and d_{pixel}=3 μm. (b) $|S_2^{ref} - S_2|$ and d_{pixel}=5 μm. (c) $|S_2^{ref} - S_2|$ and d_{pixel}=7 μm. (d) $|S_3^{ref} - S_3|$ and d_{pixel}=3 μm. (e) $|S_3^{ref} - S_3|$ and d_{pixel}=3 μm. (f) $|S_3^{ref} - S_3|$ and d_{pixel}=3 μm.

Fig. 3 demonstrates the intricate nature of light interaction in these structures. It displays the intensity pattern (S_0) in a plane parallel to the pixel at two wavelengths, in reflection along the propagation direction.

The matrix of graphs in Fig. 3 corresponds to different pixel sizes arranged along the columns, i.e. Fig. 3(a),(d), and (g) are related to the 3 μm pixel size, Fig. 3(b),(e), and (h) are related to the 5 μm pixel size, and Fig. 3(c),(f), and (i) for the 7 μm pixel size. The FF decreases along the rows from the top to the bottom, with the highest FF represented in Fig. 3(a), (b), and (c), whereas the lowest FF can be found in Fig. 3(g), (h), and (i).

Upon analysing the graphs in Figure 3, it becomes apparent that as the pixel size increases, the intensity distribution becomes more homogeneous. Additionally, the same behaviour seems to be found as the FF also increases. It is worth noting that the highest FF values can be observed in graphs (a), (b), and (c). On the other hand, the lowest FF values are seen in graphs (g), (h), and (i), which correspond to a pixel size of 3 μm. The most homogeneous intensity distribution is observed in graph (c), which corresponds to a pixel size of 7 μm and has an FF value of 94%. Conversely, the least homogeneous intensity distribution is observed in graph (g), which corresponds to a pixel size of 3 μm and has an FF value of 64%.

Following the analysis of the S_0 parameter, it is worth noting that there is an asymmetry in the intensity distribution along x, and y axis. This can be produced due to the pretilt angle and the behaviour of the LC as the voltage increases in the interpixel regions. This asymmetry is represented in different amplitude distributions on intensity along y-axis as it can be seen in Fig. 3(i) close to $y \approx 6$ μm compared to $y \approx 1$ μm in the same graph. The same behaviour can be identified on Fig. 3(h).

In Figure 4, we repeated the analysis performed in Figure 3, but this time focusing on the S_1 parameter. The figure shows the spatial variation of the S_1 parameter, and it's clear that the pixel size has a significant

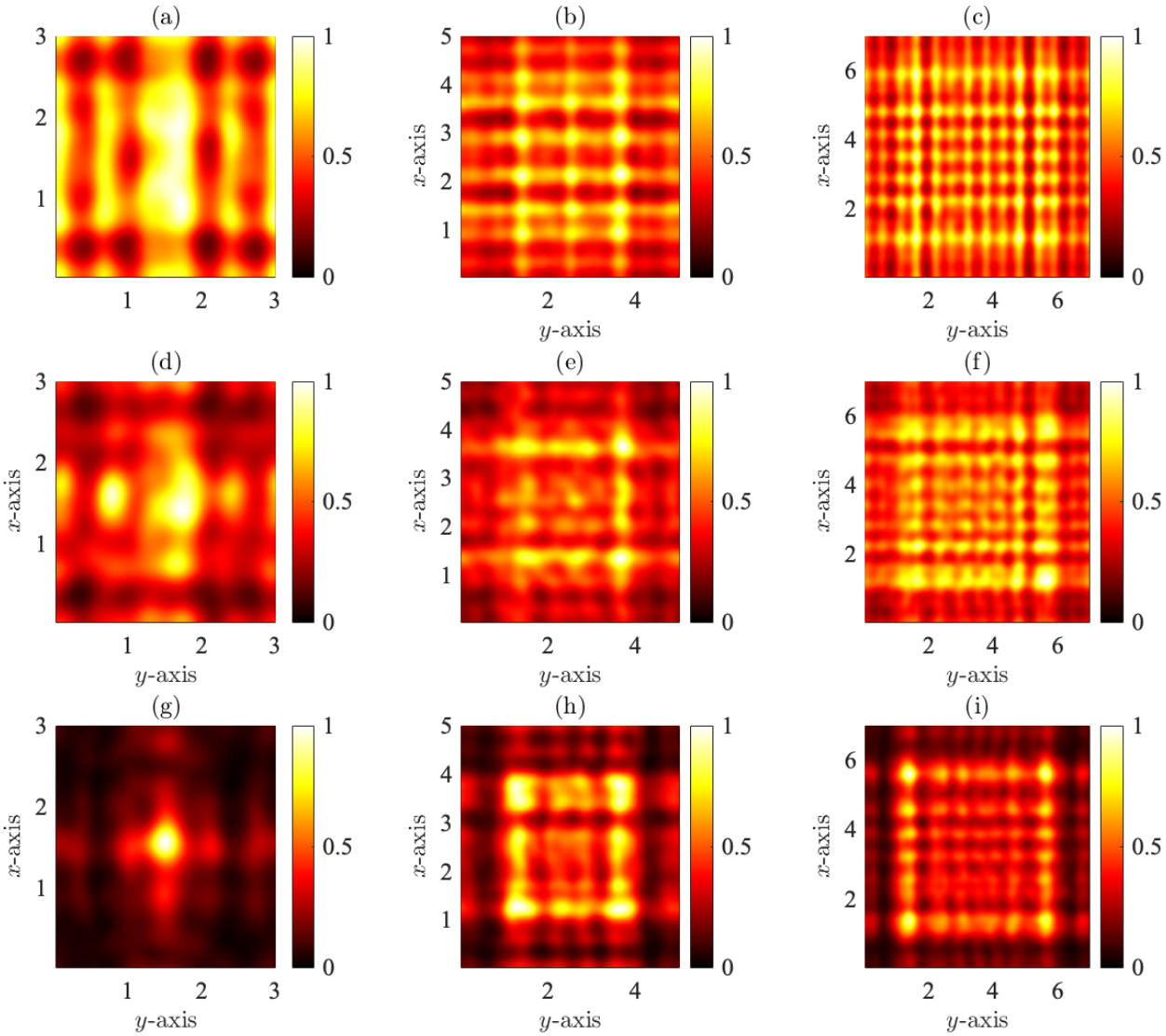

Figure 3. Representation of the Stokes parameter S_0 as a function of the voltage applied to the pixel for a spatial plane parallel to the pixel plane. (a) d_{pixel}=7 μm and FF = 94 % (b) d_{pixel}=5 μm and FF = 92 % (c) d_{pixel}=3 μm and FF = 87 % (d) d_{pixel}=7 μm and FF = 89 % (e) d_{pixel}=5 μm and FF = 85 % (f) d_{pixel}=3 μm and FF = 75 % (g) d_{pixel}=7 μm and FF = 84 % (h) d_{pixel}=5 μm and FF = 77 % (i) d_{pixel}=3 μm and FF = 64 %

influence. However, the impact of FF on the S_1 parameter is not as evident as the pixel size factor.

We observed a slightly higher level of inhomogeneity in Figure 4(g) compared to Figures 4(a) and (d) (which had a pixel size of 3 μm and a different FF). The same trend was observed for the other two pixel sizes considered, but the impact of the FF was less significant and less evident than for the smallest pixel size.

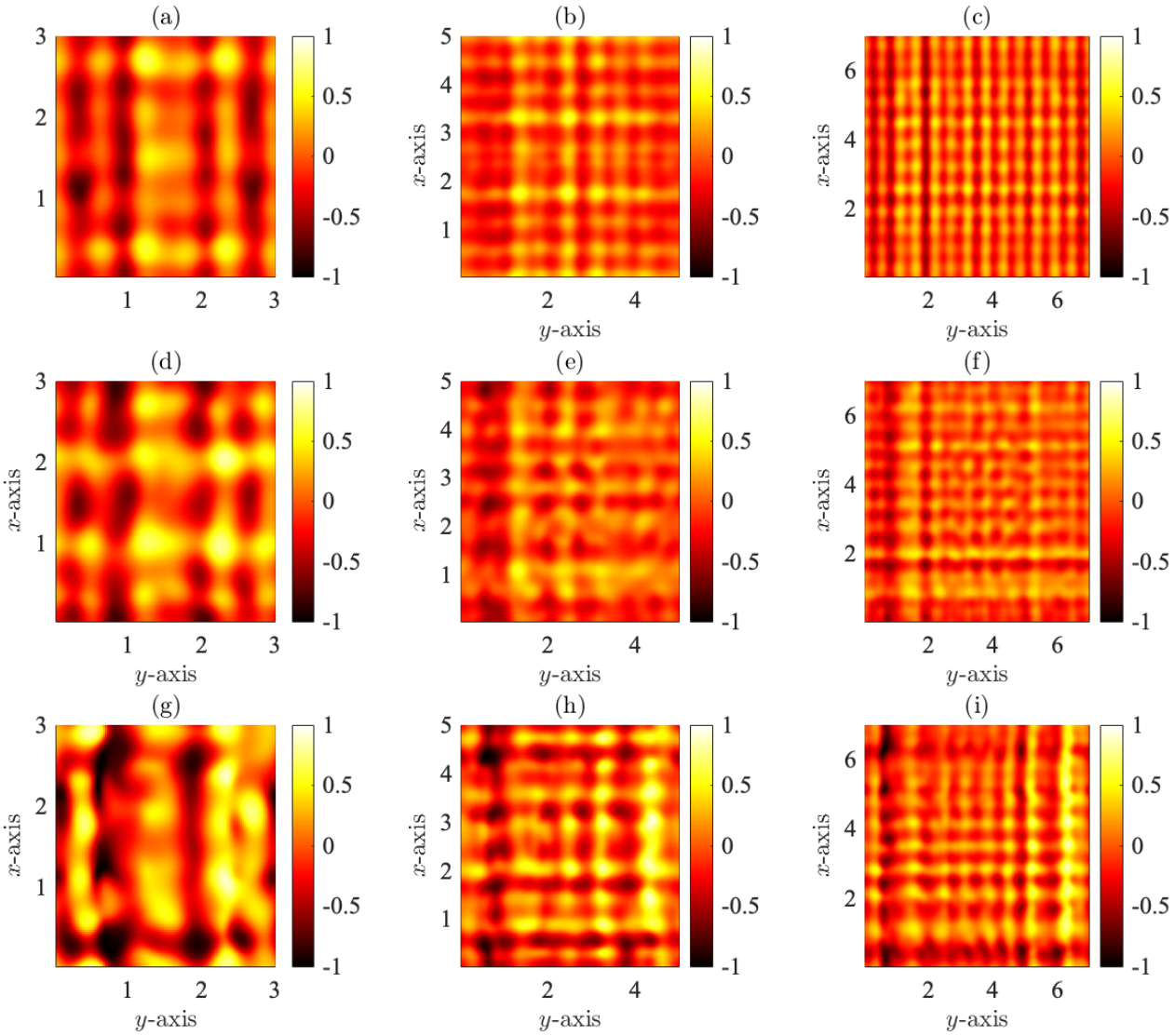

Figure 4. Representation of the Stokes parameter S_1 as a function of the voltage applied to the pixel for a spatial plane parallel to the pixel plane. (a) d_{pixel}=7 μm and FF = 94 % (b) d_{pixel}=5 μm and FF = 92 % (c) d_{pixel}=3 μm and FF = 87 % (d) d_{pixel}=7 μm and FF = 89 % (e) d_{pixel}=5 μm and FF = 85 % (f) d_{pixel}=3 μm and FF = 75 % (g) d_{pixel}=7 μm and FF = 84 % (h) d_{pixel}=5 μm and FF = 77 % (i) d_{pixel}=3 μm and FF = 64 %

4. CONCLUSIONS

In this work, we present the results of a numerical analysis of LC-SLM devices at a sub-pixel level. The study aims to examine the impact of nonlinearities, such as cross-talk between adjacent pixels, fringing fields, out-of-plane reorientation of the liquid crystal director, and diffraction effects due to the pixelated grid pattern of the microdisplay, on the Stokes parameter. The results indicate a direct relationship between pixel size and deviation of the Stokes parameters compared to infinite pixels. The influence of pixel size on the Stokes parameters varies, with S_1 being more affected by pixel size than the fill factor. Interestingly, different pixel sizes with similar or

close fill factors do not exhibit the same deviation. This disparity may be attributed to the increased relevance of the out-of-plane effect for smaller pixel sizes. However, larger pixels experience a smaller amplitude of the out-of-plane component due to the reduced area affected by the out-of-plane distribution.

For higher pixel sizes and fill factors, fringing fields and diffraction effects are the dominant factors that influence the differences between ideal and finite pixel grid cases. The interaction of pixel size and fill factor introduces intricate variations in the system's behaviour, highlighting the significance of these parameters in the device's performance. Moreover, S_2 and S_3 show a direct impact on the fill factor. However, the degree of polarisation (DOP) is consistent in all cases, and there is no depolarisation if the coherent superposition of Stokes parameters is considered in the computation process.

Further analysis is required to understand the impact of the various phenomena on the Stokes parameter. Future studies will focus on the Mueller matrix characterisation of the pixel LC-SLM and the impact of non-constant voltage setups, such as binary and staircase gratings. These analyses will give hints about the nature of the different phenomena produced in these systems regarding polarization.

Acknowledgments

The work was supported by the "Generalitat Valenciana" (IDIFEDER/2021/014 cofunded by FEDER EU program, and project PROMETEO/2021/006, GRISOLIAP/2021/106), and by "Ministerio de Ciencia e Innovación" of Spain (projects PID2021-123124OB-I00; PID2019-106601RB-I00).

REFERENCES

[1] Xiong, J. and Wu, S.-T., "Planar liquid crystal polarization optics for augmented reality and virtual reality: from fundamentals to applications," *eLight* **1**(1), 1–20 (2021).

[2] Lazarev, G., Chen, P.-J., Strauss, J., Fontaine, N., and Forbes, A., "Beyond the display: phase-only liquid crystal on silicon devices and their applications in photonics," *Opt. Express* **27**, 16206–16249 (May 2019).

[3] Maurer, C., Jesacher, A., Bernet, S., and Ritsch-Marte, M., "What spatial light modulators can do for optical microscopy," *Laser & Photonics Reviews* **5**(1), 81–101 (2011).

[4] Jesacher, A. and Ritsch-Marte, M., "Synthetic holography in microscopy: opportunities arising from advanced wavefront shaping," *Contemporary Physics* **57**(1), 46–59 (2016).

[5] Moser, S., Ritsch-Marte, M., and Thalhammer, G., "Model-based compensation of pixel crosstalk in liquid crystal spatial light modulators," *Optics Express* **27**(18), 25046 (2019).

[6] Wang, X., Wang, B., Bos, P. J., McManamon, P. F., Pouch, J. J., Miranda, F. A., and Anderson, J. E., "Modeling and design of an optimized liquid-crystal optical phased array," *Journal of Applied Physics* **98**(7) (2005).

[7] Wang, X., Wang, B., Bos, P. J., Anderson, J. E., Pouch, J. J., and Miranda, F. A., "Finite-difference time-domain simulation of a liquid-crystal optical phased array," *Journal of the Optical Society of America A* **22**(2), 346 (2005).

[8] Lingel, C., Haist, T., and Osten, W., "Optimizing the diffraction efficiency of slm-based holography with respect to the fringing field effect," *Appl. Opt.* **52**, 6877–6883 (Oct 2013).

[9] Ronzitti, E., Guillon, M., de Sars, V., and Emiliani, V., "Lcos nematic slm characterization and modeling for diffraction efficiency optimization, zero and ghost orders suppression," *Opt. Express* **20**, 17843–17855 (Jul 2012).

[10] Lu, T., Pivnenko, M., Robertson, B., and Chu, D., "Pixel-level fringing-effect model to describe the phase profile and diffraction efficiency of a liquid crystal on silicon device," *Appl. Opt.* **54**, 5903–5910 (Jul 2015).

[11] Francés, J., Márquez, A., Neipp, C., Puerto, D., Gallego, S., Pascual, I., and Beléndez, A., "Polarimetric analysis of cross-talk phenomena induced by the pixelation in pa-lcos devices," *Optics & Laser Technology* **152**, 108125 (2022).

[12] Miskiewicz, M. N., Bowen, P. T., and Escuti, M. J., "Efficient 3D FDTD analysis of arbitrary birefringent and dichroic media with obliquely incident sources," *Proc. of SPIE* **8255**, 82550W–82550W–10 (feb 2012).

[13] Bleda, S., Francés, J., Gallego, S., Márquez, A., Neipp, C., Pascual, I., and Beléndez, A., "Numerical analysis of h-pdlc using the split-field finite-difference time-domain method," *Polymers* **10**(5) (2018).

[14] Francés, J., Bleda, S., Puerto, D., Gallego, S., Márquez, A., Neipp, C., Pascual, I., and Beléndez, A., "Accurate, Efficient and Rigorous Numerical Analysis of 3D H-PDLC Gratings," *Materials* **13**(17) (2020).

[15] Yang, D. K. and Wu, S. T., [*Fundamentals of Liquid Crystal Devices*], Wiley (2015).

[16] Wang, X., *Liquid Crystal Diffractive Optical Elements: Applications and limitations*, PhD thesis, Kent State University (2005).

[17] Oh, C. and Escuti, M. J., "Time-domain analysis of periodic anisotropic media at oblique incidence: an efficient FDTD implementation.," *Optics express* **14**, 11870–84 (nov 2006).

[18] Oh, C. and Escuti, M. J., "Numerical analysis of polarization gratings using the finite-difference time-domain method," *Physical Review A* **76**(4), 043815 (2007).

[19] Roden, J., Gedney, S., Kesler, M., Maloney, J., and Harms, P., "Time-domain analysis of periodic structures at oblique incidence: orthogonal and nonorthogonal FDTD implementations," *IEEE Transactions on Microwave Theory and Techniques* **46**, 420–427 (apr 1998).

[20] Márquez, A., Martínez-Guardiola, F. J., Francés, J., Calzado, E. M., Puerto, D., Gallego, S., Pascual, I., and Beléndez, A., "Unitary matrix approach for a precise voltage dependent characterization of reflective liquid crystal devices by average stokes polarimetry," *Opt. Lett.* **45**, 5732–5735 (Oct 2020).